Ann. Geophys., 31, 45–59, 2013
www.ann-geophys.net/31/45/2013/
doi:10.5194/angeo-31-45-2013

Annales Geophysicae

ULF waves in Ganymede's upstream magnetosphere

M. Volwerk[1], X. Jia[2], C. Paranicas[3], W. S. Kurth[4], M. G. Kivelson[5], and K. K. Khurana[5]

[1]Space Research Institute, Austrian Academy of Sciences, 8042 Graz, Austria
[2]Department of Atmospheric, Oceanic and Space Sciences, University of Michigan, Ann Arbor, MI, USA
[3]The Johns Hopkins University Applied Physics Laboratory, Laurel, MD, USA
[4]Department of Physics and Astronomy, University of Iowa, Iowa City, IA, USA
[5]Institute of Geophysics and Planetary Physics, UCLA, Los Angeles, CA, USA

Correspondence to: M. Volwerk (martin.volwerk@oeaw.ac.at)

Received: 24 September 2012 – Revised: 3 December 2012 – Accepted: 5 December 2012 – Published: 7 January 2013

Abstract. Ganymede's mini-magnetosphere, embedded in Jupiter's larger one, sustains ULF (ultra-low frequency) waves that are analyzed here using data from two Galileo flybys that penetrate deeply into the upstream closed field line region. The magnetometer data are used to identify field line resonances, magnetopause waves and ion cyclotron waves. The plasma densities that are inferred from the interpretation of these waves are compared with the observations made by other plasma and wave experiments on Galileo and with numerical and theoretical models of Ganymede's magnetosphere.

Keywords. Magnetospheric physics (Planetary magnetospheres; Plasma waves and instabilities) – Space plasma physics (Waves and instabilities)

1 Introduction

Ganymede is the third Galilean moon of Jupiter and has a radius of 2631.2 km, which makes it the largest moon in the solar system. Ganymede is in a 7.115-day orbit around Jupiter, and in a 1 : 2 : 4 resonance with Europa and Io. The first Galileo flybys of this moon surprisingly showed that it possesses an internal magnetic field strong enough to create its own mini-magnetosphere inside that of Jupiter (Kivelson et al., 1996, 1998). Further investigation of all Galileo flybys has shown that not only is there an internal magnetic field, but there is a time-varying residual field after removal of the contribution of the intrinsic dipole field. The time-varying contribution can be attributed to an induced magnetic field (Kivelson et al., 2002) in a possible conducting ocean underneath the icy surface. Energetic particle data confirmed the form of the field around Ganymede by demonstrating a change in the ion and electron distributions after the crossing of the magnetopause. Loss cone distributions appeared (Williams et al., 1997b), indicating regions of half-open and closed field lines.

The presence of Ganymede's mini-magnetosphere and its closed magnetic field lines has been confirmed by close flybys of the moon. The MAG data (Kivelson et al., 1992) have shown that Ganymede's internal field near the equator is oppositely directed to the Jovian field (see e.g. Volwerk et al., 1999), and particle measurements have shown characteristic signatures of magnetospheres in low-energy electrons (Frank et al., 1997) and also at high energy where trapped electrons, radiation belts and electron beams (Williams et al., 1997a, 1998; Williams, 2001, 2004) are identified. Similarly, plasma wave observations have shown typical magnetospheric emissions (Gurnett et al., 1996). Other aspects of Ganymede's magnetosphere include auroral emissions (Barth et al., 1997; Hall et al., 1998; Eviatar et al., 2001a) and the presence of polar caps (Khurana et al., 2007), high-latitude regions from which field lines emerge but do not return to Ganymede's surface.

Studies of the Galileo data with respect to the interaction of Ganymede and the Jovian magnetosphere and the physics of Ganymede's magnetosphere and of the Jovian magnetosphere in general are important for planning JUICE, the upcoming ESA mission to Jupiter and Ganymede (see e.g. Blanc et al., 2009; Dougherty and The JUICE Science Study Team, 2011). The information that can be obtained from the earlier Galileo mission to the Jovian system can help in optimizing the specifications of the various instruments that will fly on this satellite.

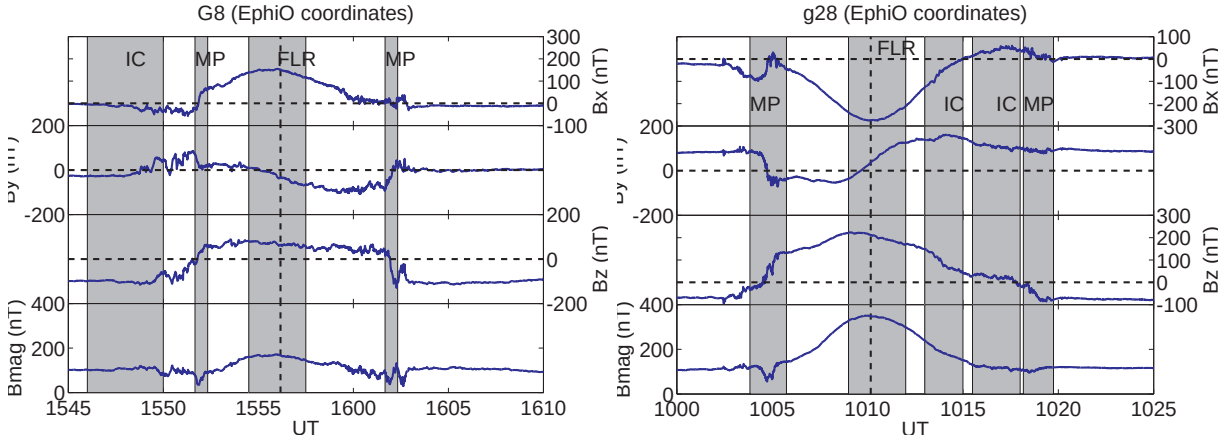

Fig. 1. Left: Galileo magnetic field data for the G8 flyby in GphiO coordinates. The GphiO coordinate system is defined as centred on Ganymede, the z-axis aligned with the rotational axis, the x-axis in the direction corotation, and the y-axis completes the triad and is mainly directed towards Jupiter. The grey filled regions are the magnetopause crossings (MP) and the intervals during which field line resonances (FLRs) and ion cyclotron (IC) waves are observed. The vertical dashed line indicates the time of closest approach. Right: the same for the G28 flyby.

In this paper we will discuss two upstream Galileo flybys of Ganymede (G8 and G28), during which the spacecraft passed close to the moon and entered into regions of closed magnetic field lines. These two flybys encountered Ganymede during two extreme locations of the moon in the Jovian current sheet. The G8 flyby has the moon near the centre of the current sheet, whereas the G28 flyby has the moon near the outer edge of the current sheet. This means that the external plasma flow around the Ganymede is drastically different. We show some of the parameters of these flybys in Table 1.

The small values of B_r, the background Jovian radial magnetic field and the centrifugal latitude for G8 show that the moon is near the centre of the current sheet (centrifugal equator) with an estimated maximum ion density of $n_i \approx 8\,\mathrm{cm}^{-3}$ (e.g. Kivelson et al., 2004). On the other hand G28 shows large B_r and centrifugal latitude indicating a significant distance from the centre of the current sheet, with an estimated ion density $n_i \approx 1\,\mathrm{cm}^{-3}$.

The difference in the ambient magnetoplasma might well cause the interaction with Ganymede's magnetosphere to be quite different for these two flybys. We will investigate the ULF (ultra-low frequency) wave activity in the neighbourhood of Ganymede along these two flybys first based on analysis of the magnetic field data and then investigate the data from other experiments (PLS (Plasma Instrumentation), PWS (Plasma Wave Spectrometer), EPD (Energetic Particle Detector)).

2 G28 FLRs near closest approach

On 20 May 2000, during the G28 flyby Galileo once more entered deeply into the upstream magnetosphere of Ganymede. Closest approach was at 10:10:10 UT at an altitude of 808.7 km, which can be mapped to an L-shell of $L \approx 1.5$. The magnetic field data, at a resolution of 3 vectors per second, for this flyby are shown in Fig. 1 (right panel). The rotation period of the spinning platform of the spacecraft was approximately 20 s. For 3 min around closest approach, Galileo remained at approximately the same L-shell, similar to the situation during the G8 flyby (see Volwerk et al., 1999). We use this interval to look for the signatures of field line resonances.

The magnetic field data are transformed into a mean field aligned (MFA) coordinate system, where the mean is determined by a low-pass filter (for periods greater than 5 min). The B_c component is along the mean field, the B_ϕ component obtained from the cross product of B_c and the radial vector to the spacecraft, describing the toroidal direction, and the B_ρ component closes the triad and is mainly in the radial direction. Spectral analysis is performed on the data (cf. McPherron et al., 1972). The data are pre-whitened (i.e. we take first differences of the time series data, which effectivity multiply the spectrum by the factor f^2 forcing the power to zero at zero frequency; see also Volwerk et al., 1999), and the spectral estimates are averaged over seven harmonics. The spectral matrix is then diagonalized for the real part (see e.g. Arthur et al., 1976). The result of the spectral density in the eigenvector system is shown in Fig. 2.

There are several spectral peaks in the red (i.e. maximum eigenvalue) component. These values are listed in Table 2. In Fig. 3 (bottom right) the detrended power spectrum (of non-pre-whitened data) is shown with the 95 % confidence level

Table 1. Various parameters for the Ganymede flybys G8 and G28. The ambient plasma environment is characterized by an ion density range $n_i = 1 - 8\,\mathrm{cm}^{-3}$ (Kivelson et al., 2004). Listed are the time of closest approach (CA), the local time (LT) of the encounter, the System III latitude (Dessler, 1983), the B_r component of the Jovian field and the dipole (centrifugal) latitude (Dip.(Cent.) Lat.), the altitude and latitude of the flyby centred on Ganymede.

	CA UT	LT hrs.	SIII Lat. deg.	B_r nT	Dip.(Cent.) Lat. deg.	alt. km	SC GLat deg.
G8	7 1997 May, 15:56:10	8.0	0.07	12	1 (1)	1603.2	28.27
G28	20 2000 May, 10:10:10	0.7	−0.10	−71	−8 (−5)	808.7	−18.96

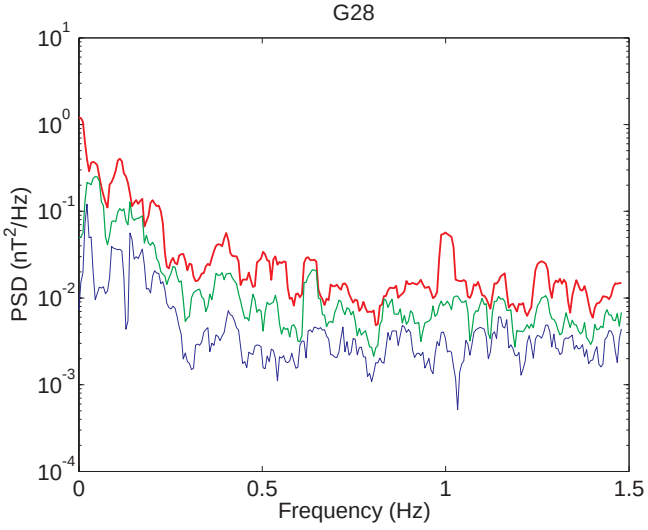

Fig. 2. The spectral density for the G28 flyby during the interval of field line resonances in the eigenvector system obtained from the real part of the cross-spectral matrix (Arthur et al., 1976), with maximum eigenvalue in red, intermediate in green and minimum in blue.

as a dashed line (see e.g. Bendat and Piersol, 1966). This shows that the first harmonic is well below the 95 % confidence level, as is the fourth harmonic. The second, third and fifth harmonics exceed the confidence level. In the top right panel, we show one of the transverse magnetic field components (B_ρ) and the band-pass filtered data for the first (red) and second (green) harmonics.

The observed peaks in the spectrum are compared to the peaks in the dipole model by Cummings et al. (1969) using the following scaling equation:

$$f_{\mathrm{model}} = f_{\mathrm{cumm}} \frac{B_{\mathrm{Gan}}}{B_{\mathrm{Earth}}} \left(\frac{L_{\mathrm{cumm}}}{L_{\mathrm{obs}}} \right)^4 \frac{\sqrt{n_{\mathrm{cumm}}}}{\sqrt{n_{\mathrm{obs}}}} \frac{R_{\mathrm{Earth}}}{R_{\mathrm{Gan}}}, \qquad (1)$$

where a mass density of $3\,\mathrm{AMU\,cm}^{-3}$ for G8 was used, and for G28 a mass density of $90\,\mathrm{AMU\,cm}^{-3}$ at $L = 1.5$ is assumed. The appropriate equatorial mass density can be found through fitting the observed harmonic spectrum with the model spectrum using Eq. (1). Ganymede's equatorial surface field strength is taken as 750 nT. It is clear from Table 2 that the measured frequencies during the G28 flyby, near closest approach, fit well with the expected model frequencies, except for the fifth harmonic.

Table 2. The first five harmonics in the spectra for G8 and G28. The model values for the FLR frequencies are obtained from Cummings et al. (1969). The boldface numbers are those frequency estimates that exceed the 95 % confidence level in the power spectrum.

Harmonic	G8 $L = 2$		G28 $L = 1.5$	
number	Obs.	Model	Obs.	Model
harmonic	Hz		Hz	
1	**0.060**	**0.059**	0.039	0.034
2	**0.211**	**0.208**	**0.116**	**0.120**
3	0.328	0.346	**0.200**	**0.200**
4	**0.468**	**0.469**	0.279	0.271
5	0.584	0.579	**0.401**	**0.334**

3 G8 revisited

Field line resonances (FLRs) were identified in the magnetometer data from Galileo's G8 flyby on 7 May 1997 by Volwerk et al. (1999). Waves were observed during the 3 min around closest approach, 15:54:47–15:57:47 UT. During this time interval the spacecraft remained on approximately the same L-shell, $L \approx 2.1$. The magnetic field data are shown in Fig. 1 (left panel). In this section we will revisit these waves and check the field line resonance interpretation. The resonance frequencies identified in the previous paper are listed in Table 2, with a comparison with the model by Cummings et al. (1969), which shows good agreement for an assumed plasma density of $3\,\mathrm{AMU\,cm}^{-3}$.

The harmonic spectrum in a principal axis system (see e.g. Arthur et al., 1976) was already shown in Fig. 6 of Volwerk et al. (1999). In Fig. 3 (left bottom) we show the detrended (third-order polynomial) power spectrum with the 95 % confidence level as a dashed line for the peaks (see e.g. Bendat and Piersol, 1966). Naturally, the data were not pre-whitened for this analysis. The first harmonic touches the 95 % confidence level, while the second and fourth harmonics are above this level of confidence, whereas the third and fifth are below. We also show one of the transverse components of the

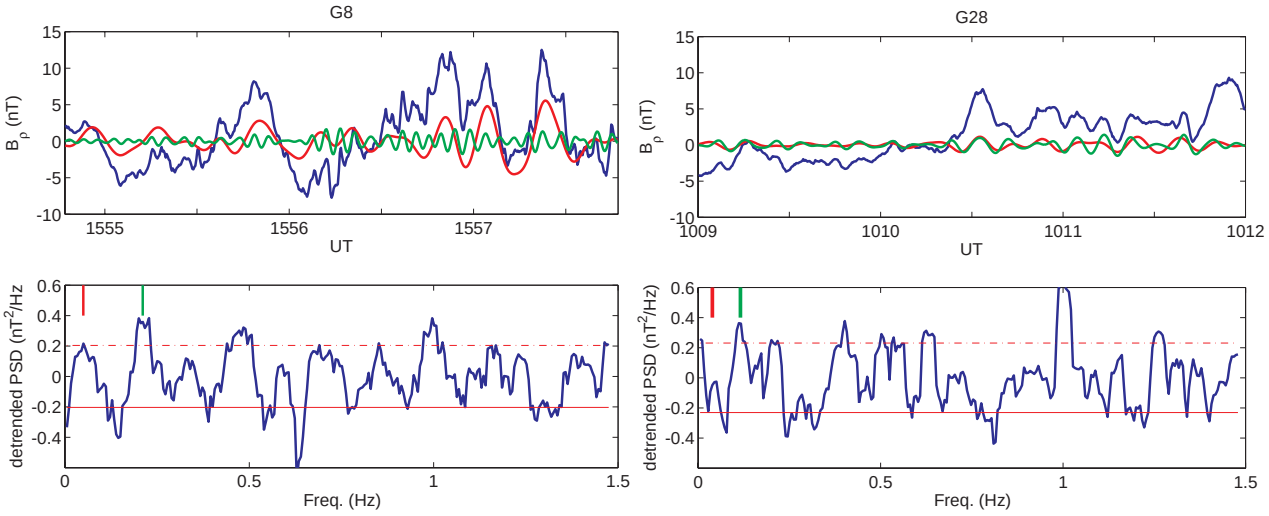

Fig. 3. Left panels: At the bottom the detrended (third-order polynomial) power spectra for the FLRs in the G8 flyby are shown. The dashed and solid horizontal red lines show the 95 % confidence levels. The small red and green lines show the location of the first and second harmonics. The top panel shows one of the transverse magnetic field components (B_ρ in blue with the band-pass filtered data for the first (red) and second (green) harmonics). Right panels: the same for G28.

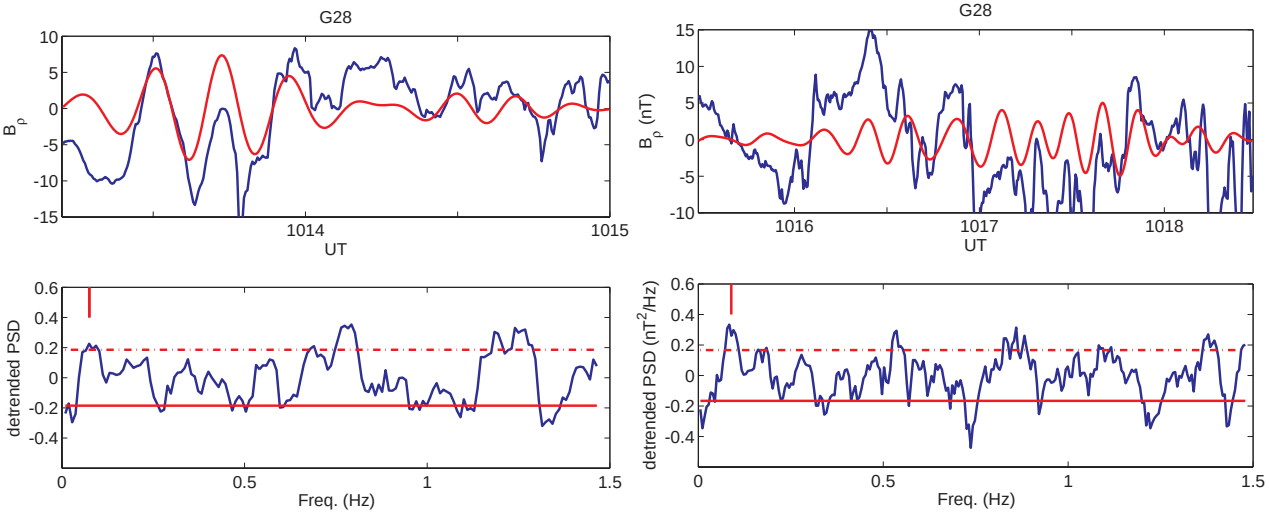

Fig. 4. At the bottom the detrended power spectrum is shown with the 95 % confidence levels for the spectral peaks. The peaks for the cyclotron waves for O_2^+ (left) and O^+ (right) are indicated by short, red, vertical lines. At the top one of the transverse magnetic field components (B_ρ) is shown in blue with superimposed band-pass filtered data (red).

magnetic field (B_ρ, top left) with superimposed band-pass filtered data for the first (red) and second (green) harmonics.

Thus, using field line resonances we obtain two estimates for the plasma density in Ganymede's magnetosphere: 3 AMU cm^{-3} at $L \approx 2$ and 90 AMU cm^{-3} at $L \approx 1.5$. Assuming that oxygen is the main heavy ion in the magnetosphere (see e.g. Calvin et al., 1996; Vasiliũnas and Eviatar, 2000; Jia et al., 2009), this would mean an ion number density of $n_\mathrm{i} \approx 0.16$ and 5.5 cm^{-3} respectively.

We have determined the plasma density at two L-shells, which allows for estimating an expected scale height of the plasma in Ganymede's magnetosphere. Assuming a simple exponential fall off,

$$n(L) = n_0 \exp\left\{\frac{L-1}{H}\right\}. \quad (2)$$

Using the above values this leads to a scale height $H \approx$ 465 km, which is about half the value determined by Gurnett et al. (1996), $H \approx 1000$ km, but closer to the value determined by Eviatar et al. (2001b) who find $H \approx 600$ km. This difference will be discussed below in Sect. 6.

4 Other wave modes

Apart from field line resonances, we have investigated the MAG data for other wave signatures for these two passes through Ganymede's magnetosphere.

4.1 Ion cyclotron waves

In Volwerk and Khurana (2010) it was shown that ion cyclotron waves near water group ion gyro frequencies (H_2O^+ or O^+) were present during the interval 15:46–15:50 UT of the G8 flyby. These waves appear on open field lines, outside of Ganymede's magnetopause (see Fig. 1, left panel). Here we seek evidence of ion cyclotron waves in the MAG data for G28. During the interval of 10:15:30–10:18 UT, the spacecraft is at relatively constant magnetic field strength and results from global MHD (magnetohydrodynamics) simulation of the magnetosphere (Jia et al., 2010) and EPD data (Williams, 2001) show that the spacecraft is on open field lines. In Fig. 4 (bottom right) we show the detrended power spectrum for this interval with the 95 % confidence level indicated by a dashed line.

The first peak in the spectrum at ∼89 mHz is left-hand polarized at ∼80 %, and with the average local magnetic field strength $|B| = 116 \pm 8$ nT. Assuming an ion cyclotron wave, this would correspond to ions with $m_i \approx 20 \pm 1$ AMU. However, it is not unusual that the emitted cyclotron waves are up to 80 % below the actual gyro frequency (see e.g. Lee, 1989; Mazelle et al., 2004). The resonance condition for ion cyclotron waves is given by

$$\omega - \boldsymbol{k} \cdot \boldsymbol{v}_{\parallel} = \pm n \Omega_i, \tag{3}$$

where ω and $\boldsymbol{k}$ are the wave frequency and vector, $\boldsymbol{v}_{\parallel}$ the parallel velocity of the ions along the magnetic field and Ω_i the ion cyclotron frequency. The thermal background plasma impedes the growth of the waves at the ion cyclotron frequency. However, waves travelling at a small angle with respect to the magnetic field can grow at frequencies below Ω_i as well as waves emitted by particles with a small parallel velocity.

This would bring the ion mass to $m_i \approx 17 \pm 1$ AMU. This is close to the weight of the water group ions also observed in G8. In Fig. 4 top right panel, one of the transverse components of the magnetic field (B_ρ) is shown with the band-pass filtered data superimposed.

Slightly earlier, during the interval of 10:13–10:15 UT, there is strong transverse wave power at a frequency of ∼75 mHz, which is ∼80 % left-hand elliptically polarized. The detrended power spectrum is shown in Fig. 4 bottom left. These waves occur on open field lines as apparent from the single energetic particle loss-cone that will be shown below in the discussion of the EPD data. The averaged magnetic field strength during this interval is $|B| = 182 \pm 20$ nT. Assuming the waves are cyclotron waves, this would lead to an ion mass of $m_i \approx 37 \pm 4$ AMU. Taking into account the emission below the local gyro frequency, this leads to a mass $m_i \approx 30 \pm 4$ AMU. This would indicate the presence of O_2^+ ions.

The presence of the ion cyclotron waves can be used to estimate the ion pick-up rate (see e.g. Gary, 1991; Huddleston and Johnstone, 1992; Volwerk et al., 2001; Cowee et al., 2007; Delva et al., 2008a, for application in different space environments). Basically, part of the energy in the ring distribution of the pick-up ions can be released into cyclotron wave energy if the energy of the ring well exceeds the thermal energy of the background plasma, which is indeed the case with an exospheric ion temperature of ∼450 K (Barth et al., 1997) and a pick-up velocity of 50 to 100 km s^{-1}. The free energy in the ring (E_{fr}) is given by

$$E_{fr} = 0.5 m_r n_r v_{pu}^2 \phi, \tag{4}$$

where m_r and n_r are the mass and density of the pick-up ions in the ring and v_{pu} is the pick-up velocity. The efficiency factor ϕ is usually around 0.3 (Cowee et al., 2007).

When we assume that the free energy in the ring is transformed to wave energy of the cyclotron waves, it is possible to calculate the number density of the ring n_r through determination of $(\delta B)^2$, the squared amplitude of the waves. This can be estimated from the power spectrum:

$$(\delta B)^2 = \int_{f1}^{f2} P(f) df, \tag{5}$$

where $P(f)$ is the power spectral density (PSD) in nT^2 Hz^{-1} and the limits of the integral $f1$ and $f2$ can be set at the cyclotron frequency $f_c \pm$ the half width at half maximum (HWHM) of the spectral peak. From that the density in the pickup ring is found through equaling the free energy to the wave energy $E_w = (\delta B)^2 / 2\mu_0$ (see also Huddleston et al., 1998; Volwerk et al., 2001; Cowee et al., 2007; Delva et al., 2008a):

$$n_r = \frac{E_w}{\phi m_r v_{pu}^2}. \tag{6}$$

For the O^+ cyclotron waves, the PSD shows for G8 a peak of $10^{2.239}$ nT^2 Hz^{-1} at a frequency of $f_c = 96$ mHz and HWHM = 25 mHz and for G28 a peak of $10^{2.344}$ nT^2 Hz^{-1} at a frequency of $f_c = 89$ mHz and HWHM = 33 mHz. This leads to a wave energy of $E_w \approx 4 \times 10^{-12}$ J. With the pick-up velocity at $v_{pu} \approx 100$ km s^{-1} outside the magnetopause for G8, this leads to a pick-up density of $n_r \approx 1$ cm^{-3}. For G28, inside the magnetopause, the pick-up velocity is lower at $v_{pu} \leq 50$ km s^{-1}, which would imply a pick-up density, i.e. the density of the ions in the ring distribution, of $n_r \geq 4$ cm^{-3}.

For the cyclotron waves generated by heavier O_2^+ ions in the G28 flyby, the spectral power density is $10^{2.529}$ nT^2 Hz^{-1} at a frequency of $f_c = 75$ mHz and HWHM = 25 mHz, which corresponds to an energy of $E_w \approx 5 \times 10^{-12}$ J. Assuming a

pickup of 50 km s^{-1}, this leads to a pick-up density of $n_r \approx 2.5\,\mathrm{cm}^{-3}$.

As was done in Volwerk et al. (2001), this pickup density will be transformed to a pickup rate:

$$\dot{N} = A v_{pu} n_r, \tag{7}$$

where A is an effective surface through which the pickup ions are lost. The width Δy of the surface perpendicular to the flow can be estimated by the region over which the waves are observed, giving $\Delta y \approx 0.75$ and $0.5\,R_G$ for O_2^+ and O^+ respectively. The height Δz of this surface is unknown, but we will set to $1\,R_G$ for convenience. This leads to pickup rates $\dot{N} \approx 5 \times 10^{23}\,\mathrm{s}^{-1}$ for each species.

4.2 Magnetopause waves

For the G8 flyby, the main power on the closed field lines is in the FLRs. However, there is also strong wave power connected to the magnetopause crossings. This has already been addressed by e.g. Kivelson et al. (1998), where it was posited that the strong oscillations of the field before crossing the magnetopause were Kelvin–Helmholtz waves, as in a minimum variance coordinate system (Sonnerup and Scheible, 1998) B_m and B_n vary in phase, whereas B_l is in quadrature. Jia et al. (2010) provide a different interpretation. They have modelled the magnetopause and shown that, even under steady upstream conditions, reconnection at Ganymede's magnetopause is intermittent rather than steady, and consequently the location of the magnetopause in their simulation varies in time, giving the appearance of waves on the boundary. The calculated locations of the magnetopause during the simulation do not follow completely the whole increased B_y region observed just before magnetopause entrance. However, they also show that the bursty reconnection on the upstream magnetopause produces FTEs (flux transfer events) that are transported downstream. When transported along the sides of the magnetosphere, the FTEs produce signatures in the MAG data of "folded" flux tubes passing over the spacecraft. Such folded flux tubes moving downstream would produce rotations of the field, mainly in the $B_y - B_z$ components.

In Fig. 5 the magnetic field data around the G8 magnetopause crossings are shown in the GphiO coordinate system and in a magnetic field aligned system. In the left panels, showing the inbound magnetopause crossing, the main oscillations in the field are in B_ϕ with peak-to-peak amplitudes of $\Delta B_\phi \approx 60$ nT. The ϕ direction corresponds to the B_y direction of the GphiO coordinate system. There is little variation in the total magnetic field strength $\Delta B_{mag} \leq 14$ nT, which means that these are mainly field rotations. The period of these fluctuations varies between 20 and 40 s.

For the inbound crossing, the main variations are from the mean field aligned component B_θ into the transverse components B_ϕ and B_r and these rotations are shown in a hodogram and the inclination angle of the field (in Fig. 6 (top left)):

$$\alpha = \mathrm{atan}\left\{B_\theta / \sqrt{B_\phi^2 + B_r^2}\right\}$$

There is little compression of the field. We have plotted the same quantities for the data in GphiO coordinates in the bottom left panels of Fig. 6. The strong rotations of the field shown in Fig. 5 are colour coded. The red/green/blue rotations clearly make a circular motion, whereas the cyan "rotation" (inside the magnetopause boundary) seems more linearly polarized.

The inclination angle remains high, most of the time $\alpha \geq 70°$, indicating that the field remains mainly along the mean average field. The data in GphiO coordinates show that the inclination angle

$$\gamma = \mathrm{atan}\left\{B_z / \sqrt{B_x^2 + B_y^2}\right\} \geq -70°,$$

indicating a tilted magnetic field with respect to the Jovian rotation axis, which is expected for draped field lines in the neighbourhood of Ganymede.

During the outbound crossing of the magnetopause, there are large oscillations in the field, as shown in the right panels of Fig. 5, similar as during the inbound crossing. However, these oscillations are connected with a much stronger compressional component with $\Delta B_{mag} \approx 50$ nT. The period of these waves is around 90 s.

The hodograms of the transverse components of the magnetic field during the outbound crossing are shown in Fig. 6 right panels. The variation in the hodogram is not as nicely circular as in the inbound case; there is much stronger variation in the $B_\theta(B_z)$ component, which is also reflected in the change in B_{mag} for these rotations. The elevation angle is on average greater than in the inbound case around $\alpha \approx 60°$, in agreement with the more compressional nature of the oscillations. In the GphiO coordinate system, the first 15 s the field is little bent back. However, afterwards the field is strongly bent back with $\gamma \approx -50°$, and then the field returns to not being bent back.

We also look at the data around the magnetopause crossings during the G28 flyby in Fig. 7. The first noticeable difference with the G8 flyby is that, outside the magnetopause, the oscillations of the field are much smaller, and during the outbound phase of the flyby the interesting oscillations are in the grey magnetopause region. Very interesting are the small sharp structures observed between 10.04 and 10.06 h before entering the magnetopause, which seem to have bipolar structure in B_r and monopolar in B_ϕ, not unlike the signature of flux tubes. They have a duration of several seconds and could well be evidence for the FTEs created by reconnection at the magnetopause as discussed above.

Once more we study the field variations in hodograms and inclination angles. There is little variation in the inclination angle $\alpha \geq 80°$, indicating little rotation from mean field aligned into transverse components. The inclination

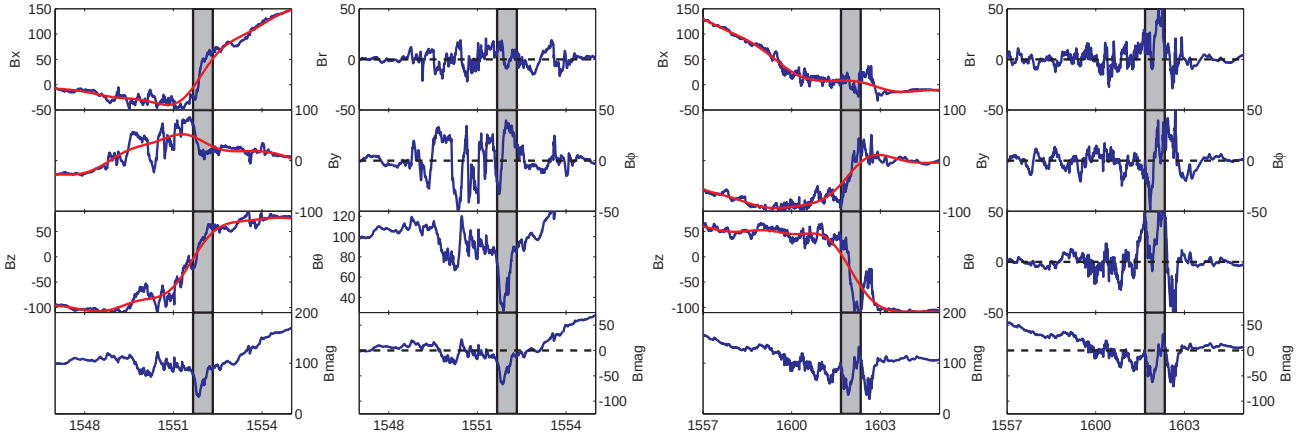

Fig. 5. Left: G8 inbound magnetopause crossing in GphiO coordinates (with the data in blue and the low-pass filtered data in red superposed) and in mean field aligned coordinates. The grey shaded area is the magnetopause crossing. Right: the same for the G8 outbound magnetopause crossing.

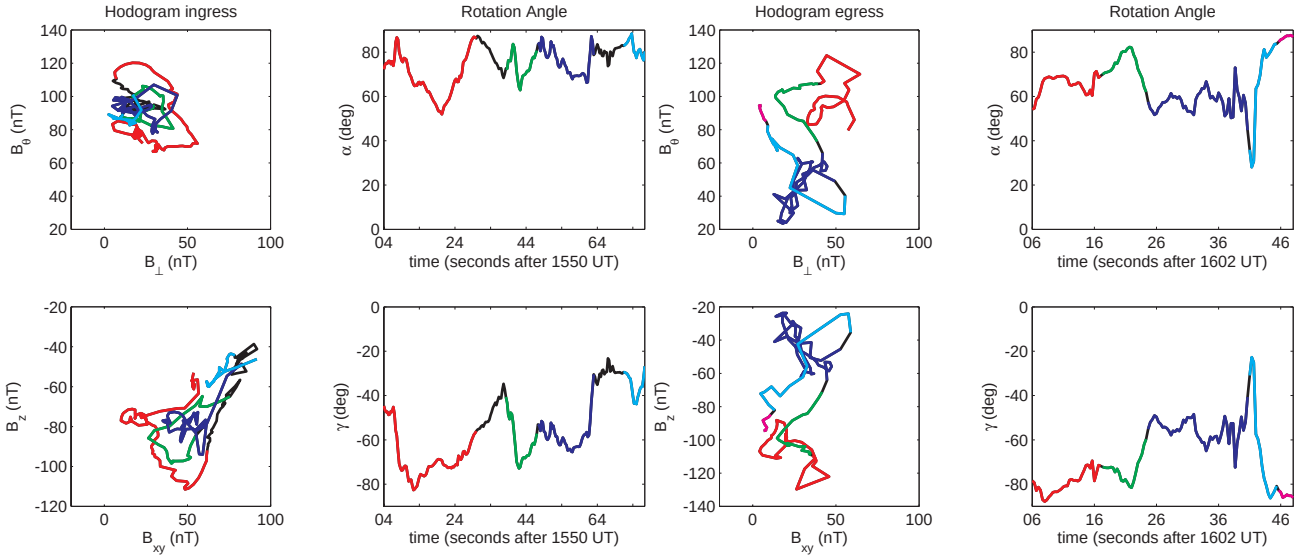

Fig. 6. Left: G8 inbound magnetopause crossing hodogram for the interval 15:50:04–15:51:24 UT. Right: the same for the G8 outbound magnetopause crossing for the interval 16:02:06–16:02:48 UT.

angle $\gamma \geq -40°$ shows that the field becomes more draped as Galileo gets closer to the magnetopause.

The hodograms show that the oscillations are not as nicely ordered as in the G8 inbound case. Before entering the magnetosphere there are slight rotations of the field from field aligned to transverse (see Fig. 8 left panels). However, the main oscillations are transverse at no specific period. That is even more the case when exiting the magnetosphere (see Fig. 8 right panels). However, the period of the first few oscillations is close to the period of the ion cyclotron waves just inside the magnetosphere and can well be created by pickup ions "leaking through" the magnetopause.

As already mentioned the big difference between the two flybys is that G8 occurred whilst Ganymede was near the centre of the current sheet, whereas during G28 the moon was located near maximum magnetic latitude outside of the current sheet. This will be discussed further below in Sect. 6.

5 Comparison with other data

We can compare the results inferred from the magnetometer observations, e.g. the density results, with the particle/plasma measurements of the PLS plasma instrument (Frank et al., 1992), the PWS plasma waves instrument (Gurnett et al., 1992) and the EPD energetic particle detector (Williams et al., 1992).

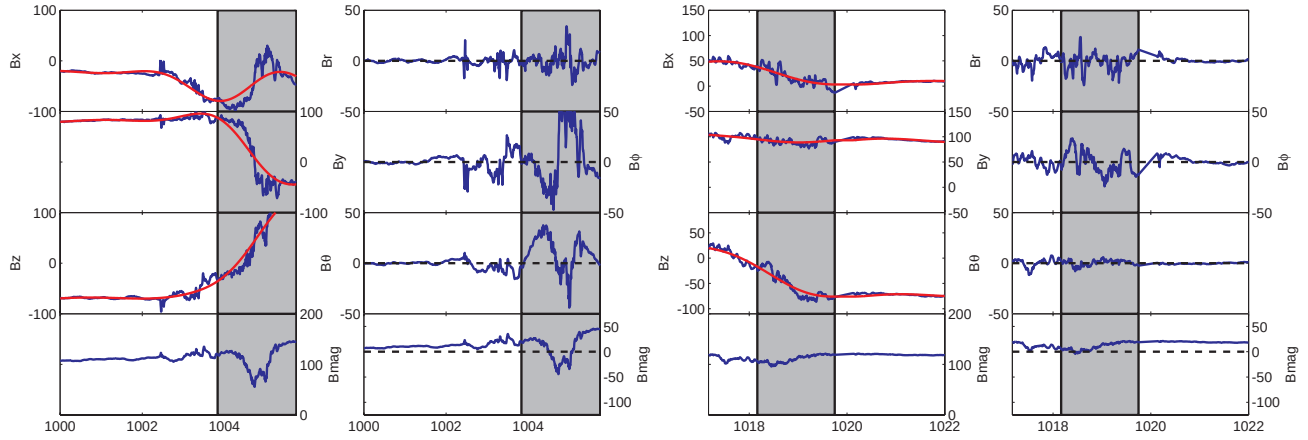

Fig. 7. Left: G28 inbound magnetopause crossing in GphiO coordinates (with the data in blue and the low-pass filtered data in red superposed) and in mean field aligned coordinates. The grey shaded area is the magnetopause crossing. Right: the same for the G28 outbound magnetopause crossing.

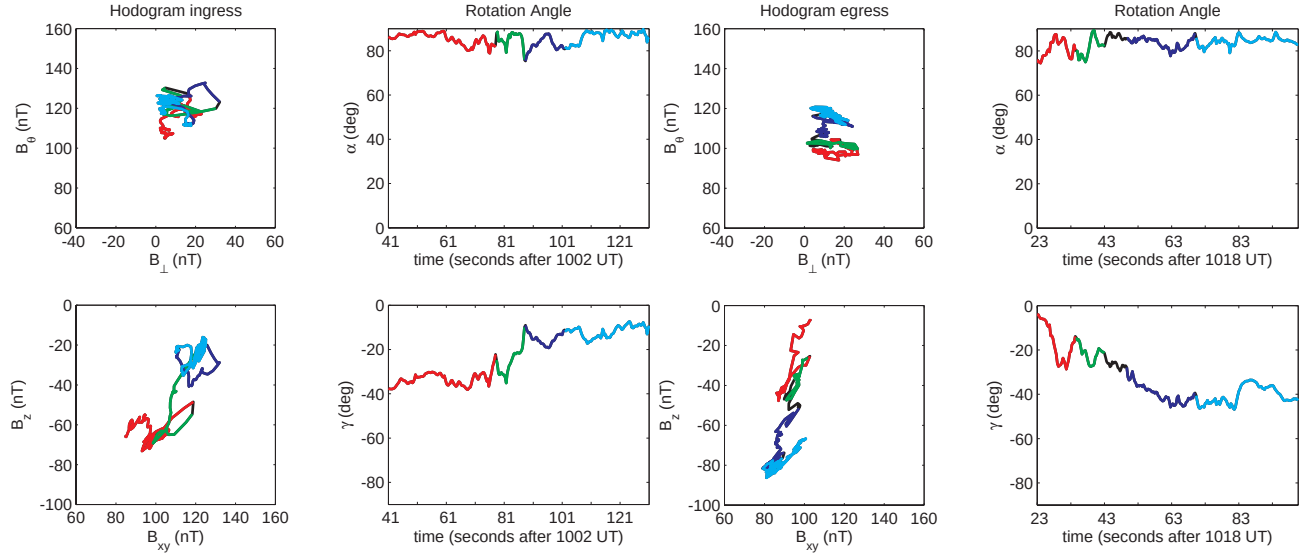

Fig. 8. Left: G28 inbound magnetopause crossing hodogram for the interval 10:02:40–10:04:12 UT. Right: the same for the G28 outbound magnetopause crossing for the interval 10:18:23–10:19:42 UT.

5.1 PLS

In Fig. 9 we show the energy spectrograms for the G8 and G28 flybys (energy spectra obtained from the Planetary Data System). The count rate is low for both of the two flybys near closest approach. However, our estimates from the FLRs showed a higher density for G28 than for G8. So why does the PLS not show different count rates?

In order to understand this difference between the density estimates and the count rates in the PLS data, we turn to Eviatar et al. (2001b), who discussed the ionosphere of Ganymede, based on an earlier paper (Eviatar et al., 1964). They derive a density distribution for the magnetosphere given by

$$\frac{n(r,L)}{n(1,L)} = \left(1 - \sqrt{1-\frac{B}{B_0}}\exp\left\{\frac{-\beta B(1-\frac{R_{\rm Gan}}{r})}{B_0 - B}\right\}\right) \exp\left\{-\beta\left(1-\frac{R_{\rm Gan}}{r}\right)\right\}, \quad (8)$$

where $\beta = mv_\infty^2/2k_{\rm B}T$, and we can set $v_\infty \approx 2740\,{\rm m\,s^{-1}}$ as the escape velocity. A realistic temperature range for Ganymede's ionosphere was found to be $150 \le T_{\rm i} \le 500\,{\rm K}$ (Eviatar et al., 2001b). Using all these values we find a range for β of $50 \ge \beta \ge 15$. The observed density ratio is $n(1.5)/n(2) \approx 27$ for which $\beta \approx 20$ or $T_{\rm i} \approx 360\,{\rm K}$. The temperature inferred for the exosphere is of the order of 0.03 eV, a temperature that falls well outside the specifications of the

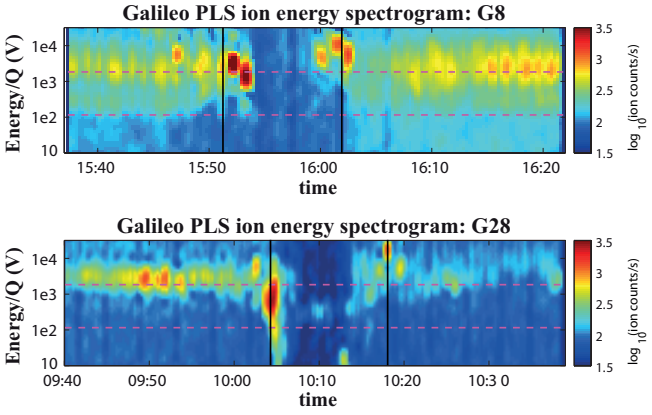

Fig. 9. Ion energy spectrograms measured by the Galileo PLS during the G8 (top) and G28 (bottom) flybys. The colour-coded ion counting rate represents the maximum response at a given E/Q during one spacecraft spin period. In each plot, two horizontal dashed lines mark the mean energies for two ion masses (top line for 16 AMU and bottom for 1 AMU) determined for a given velocity of the ambient Jovian flow (150 km s^{-1}). The PLS data were obtained from the PPI node of the Planetary Data System.

PLS instrument (Frank et al., 1992). Barth et al. (1997) arrive at a slightly higher exospheric temperature of 450 K, using Galileo ultraviolet observations.

The pickup ions discussed above are at higher energies than the thermal plasma on the closed field lines. The pickup results in heavy ions at an energy around 940 eV, which one should be able to identify in the energy spectra. In Fig. 9 top panel, there is an increased count rate of O^+ (upper dashed line) during the interval 15:46–15:50 UT, during which ion cyclotron waves were observed in the G8 flyby. This is at an $E/Q \sim 2 \times 10^3$ V, which corresponds to the energy of oxygen ions at a velocity of 150 km s^{-1}, higher than the assumed 100 km s^{-1} pickup velocity above. However, the maximum velocity of the particles for pickup in the spacecraft frame is twice the flow velocity (see e.g. Coates and Jones, 2009, $v_{\mathrm{pu,\,max}} = 2v_{\mathrm{sw}} \sin\theta$ with $\theta = \angle(\boldsymbol{B}, \boldsymbol{v})$). Thus the increased counts at higher energy than the red line could be from pickup ions. However, these are omnidirectional spectra, whereas pickup ions are usually identified by studying the appropriate sectors of the PLS instrument (see e.g. Paterson et al., 1999, for pickup ions near Europa). Lately, a re-investigation has started of the PLS data near Ganymede, and for the G8 flyby it was shown that there was evidence in the PLS data for pickup ions outside the magnetopause (W. R. Paterson, private communication, 2012).

Also in the G28 spectrogram there is a indication of increased counts during the interval 10:15–10:20 UT, during which the O^+ cyclotron waves were observed.

5.2 PWS

Another instrument capable of deducing the plasma density is PWS, where often the upper hybrid frequency can be used to determine the electron density (see e.g. Kurth et al., 2001, for electron densities near Europa). In Fig. 10 the PWS spectrograms are shown for the G8 and G28 flybys. In a white line the electron gyro frequency is shown. There is no upper-hybrid signature in the spectrograms that might be used to deduce the electron density. During the G8 flyby there is no nKOM cut-off observable to deduce an electron density. There is, however, at ∼16:03 UT a weak narrow-band radio emission (in the black box in Fig. 10 left panel) near ∼25 kHz. This signature corresponds to an electron density $n_{\mathrm{e}} \approx 8\,\mathrm{cm}^{-3}$. However, note that the cut-off frequencies that are determined give an upper limit to the electron density in the magnetosphere, but not necessarily at the location of the spacecraft.

During the G28 flyby there are two locations where there is a nKOM cut-off: around ∼10:10 UT (closest approach) at ∼74.3 kHz and around ∼10:15 UT at ∼57.7 kHz, both marked by a black line in Fig. 10 right panel. These two cut-offs translate into electron densities $n_{\mathrm{e}} \leq 68\,\mathrm{cm}^{-3}$ and $n_{\mathrm{e}} \leq 41\,\mathrm{cm}^{-3}$ respectively. There is also an interval of radio emission around ∼10:13 UT (marked with a black box in Fig. 10 right panel), which can be interpreted as the upper hybrid frequency at ∼28.571 kHz, which would correspond to an electron density $n_{\mathrm{e}} \approx 9.5\,\mathrm{cm}^{-3}$.

How should these PWS results be interpreted in view of the inferred densities from the FLRs? In general it is assumed (as in Volwerk et al., 1999) that the charge per ion is 1.5, which means that the electron density is ∼1.5 times the ion density.

Galileo observations presented by Gurnett et al. (1996) for the G1 (downstream and high latitude) flyby indicate a high-density ionosphere with a maximum density of 100 particles cm^{-3} and a scale height of 1000 km. Further investigations by Eviatar et al. (2001b), including also the G2 (polar) flyby, showed good agreement between the two radial electron density profiles. This is in reasonable agreement with the maximum electron densities that have been determined above, considering there may be an upstream-downstream asymmetry in the magnetosphere.

The upper-hybrid emissions seen in G28 correspond to an electron density $n_{\mathrm{e}} \approx 9.5\,\mathrm{cm}^{-3}$, and at ∼10:13 UT Galileo is at $R \approx 1.5\,R_{\mathrm{G}}$. This is outside the interval where the FLRs were measured, however. The FLRs showed a number density (assuming oxygen to be the main ion) $n \approx 5.5\,\mathrm{cm}^{-3}$, which together with a charge per ion of 1.5 would underestimate the electron density, but is in the right ball park.

The narrow-band radio emission seen in G8 could correspond to an electron density $n_{\mathrm{e}} \approx 8\,\mathrm{cm}^{-3}$ at ∼16:03 UT. This, again, is outside the interval where the field line resonances were observed and a number density of $n_{\mathrm{i}} \approx$

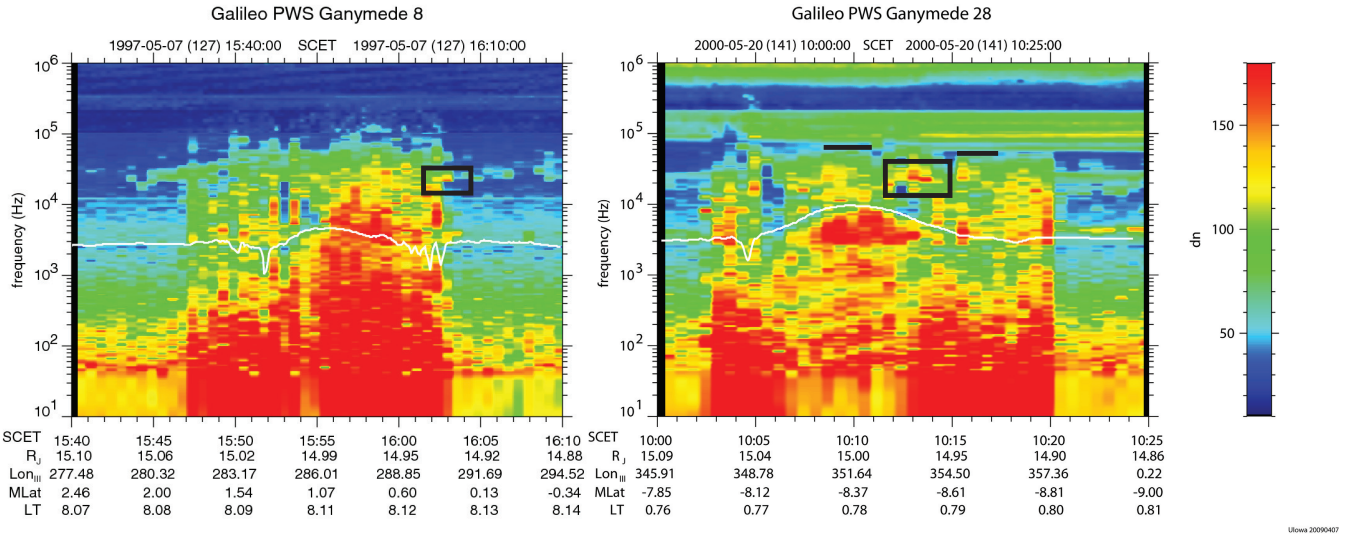

Fig. 10. The PWS spectrograms for G8 (left) and G28 (right) flybys. The black boxes in both panels indicate narrow band radio emissions, and the black lines in the right panel show the nKOM cut-off.

$0.16\,\mathrm{cm}^{-3}$ was inferred. Quite possibly, the spacecraft was already outside of Ganymede's magnetosphere at this time.

5.3 EPD

The location of the magnetopause crossing can be established unambiguously at low latitudes on the day side by using energetic particle properties to identify the boundary between ambient flux tubes and closed flux tubes of Ganymede's magnetosphere. For this purpose we study four different channels of the EPD data: B1 (electrons), T02 (oxygen $416 \leq E \leq 816\,\mathrm{keV}$), T03 (oxygen $816 \leq E \leq 1792\,\mathrm{keV}$) and A1 (mixed ions: H, He, O, S). These data can be used e.g. to find whether Galileo is on open or closed field lines, using the pitch angle distribution of the particles. In Fig. 11 the EPD data are shown for G8 (15:40–15:57 UT) and G28 (10:05–10:24 UT). The format of the scans is longitude and latitude of the detection sphere with the pitch angle of the particles given as contours, and the counts are depicted by the colour bar.

For G8 the interval 15:40:03–15:57:22 UT is shown in Fig. 11 top panel. Williams et al. (1997a) show that the electron loss-cone signatures were observed from ∼15:52 to ∼16:00 UT. This shows that indeed during the interval of field line resonances (15:54:47–15:57:47 UT) the spacecraft was on closed field lines. Before entering the region of closed field lines, 15:46–15:50 UT, ion cyclotron waves were observed in the MAG data near the O^+ or H_2O^+ gyro frequencies (Volwerk and Khurana, 2010). The EPD data for G8 during this interval are marked by a purple box in Fig. 11. The data show only partial ring distributions for O in the T02 channel with maxima around parts of the 90° contours. There is a minimum in the anti-parallel direction, indicating one foot point connected to the moon. The T03 channel shows more fully developed, but still partial ring distributions. This partial ring could be related to the gyro radius of the energetic ions. The gyro radius for the T02 channel is 3280–4599 km (1.25–1.75 R_G) at a magnetic field strength of ∼120 nT. At the location at which the cyclotron waves were observed, Galileo was at a radial distance greater than 2 R_G, so there cannot be a shadowing effect of the moon in this energy range. For the T03 channel the energy range is higher and thus the the gyro radius larger. Here there could be a shadowing effect by the moon.

For G28 the interval 10:05:09–10:24:28 UT is shown in Fig. 11 bottom panel. Williams (2001) show that trapped-like electrons exist during the interval ∼10:06–10:12 UT and trapped ions during ∼10:08:30–10:12 UT, giving an indication of the closed field line region. The interval during which the FLRs were observed, 10:09–10:12 UT, fits well with these values. The interval that the ion cyclotron waves are observed is indicated by the purple box (∼10:15–∼10:19 UT), i.e. well outside the closed field line region. The energetic oxygen looks ring-like around 90° pitch angle. There is evidence for a single loss cone in the anti-parallel direction, which agrees with Galileo being in the other Ganymede hemisphere as during the G8 flyby.

Ion cyclotron waves are often associated with ring distributions often created by ion pickup (see e.g. Lee, 1989; Huddleston and Johnstone, 1992; Mazelle et al., 2004; Delva et al., 2008b). In the case of Ganymede freshly ionized oxygen would be picked up at a velocity of $\sim 100\,\mathrm{km\,s}^{-1}$, which would correspond to an energy of $E \approx 940\,\mathrm{eV}$, which is well below the energy of the oxygen measured by the EPD.

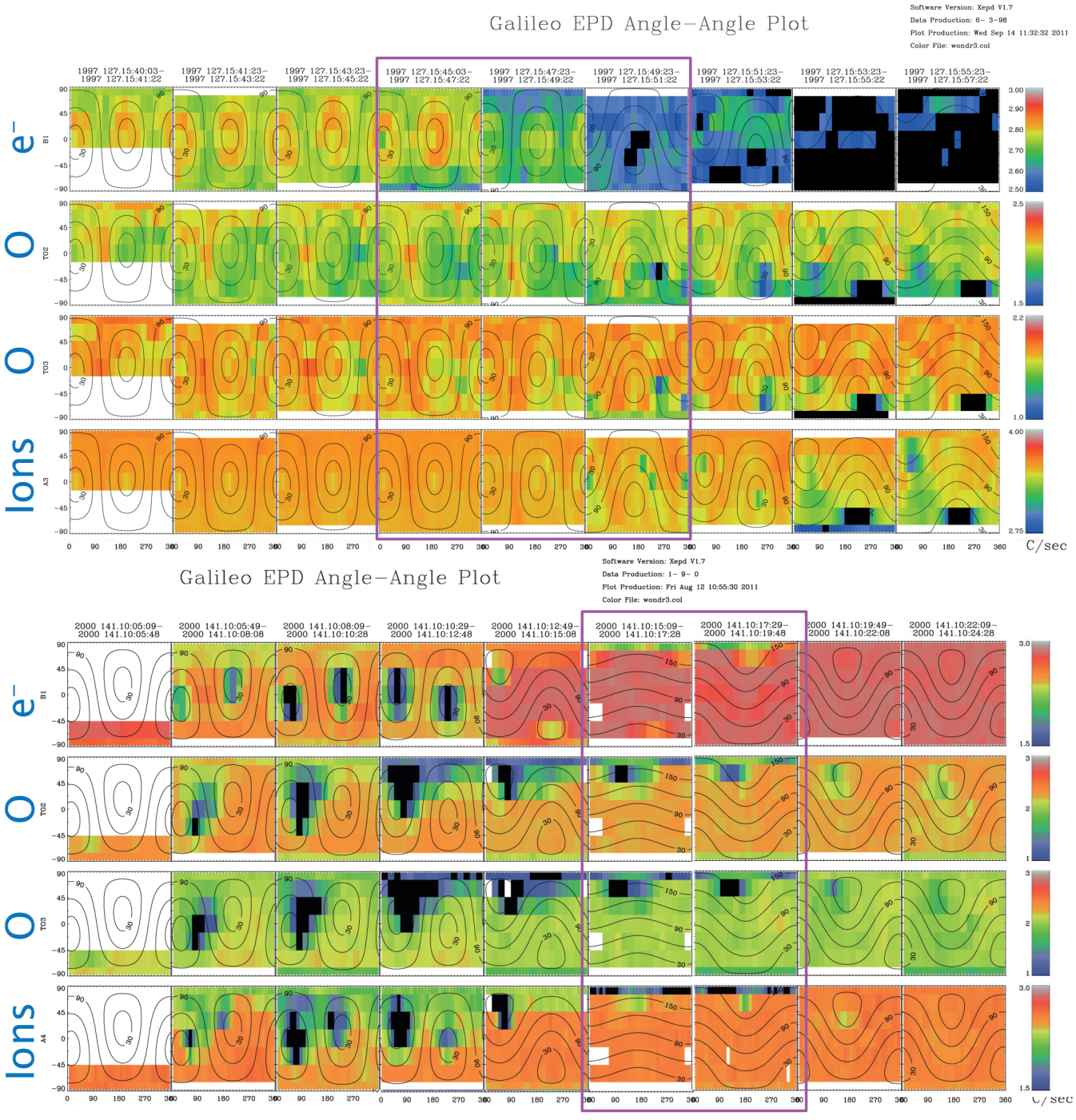

Fig. 11. The EPD energetic particle data for G8 (top) and G28 (bottom). Shown are the electron (B1 $1.5 \leq E \leq 10.5$ MeV), oxygen (T02 $416 \leq E \leq 816$ keV, T03 $816 \leq E \leq 1792$ keV) and ion data (A1 $42 \leq E \leq 65$ keV for protons). The format per small panel is longitude and latitude of the detection sphere with the pitch angle of the particles given as contours and the counts are depicted by the colour bar. The purple boxes indicate the intervals for which ion cyclotron waves are observed in the MAG data.

6 Discussion

We have investigated the Galileo data obtained during two flybys of Ganymede's upstream low-latitude magnetosphere focusing on the interpretation of various kinds of wave modes that are present. Combining the MAG data with those from other instruments (PLS, PWS and EPD) enhances the interpretation of the wave modes and their inferred physical parameters, such as the local plasma density. In Fig. 12 we show the location of the observed ULF wave modes

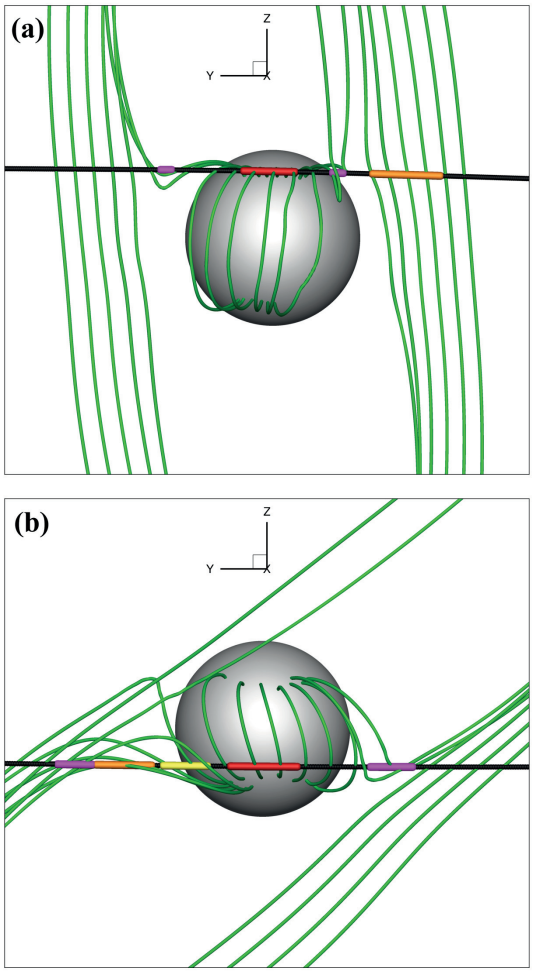

Fig. 12. A overview of the location of the various ULF wave modes along the two flybys: **(a)** G8 and **(b)** G28. The field line resonances are in red, the O^+ cyclotron waves in orange, the O_2^+ cyclotron waves in yellow and the magnetopause waves in purple. Magnetic field lines are traced along the orbits and shown in green, which are obtained from the numerical model of Jia et al. (2009).

along the orbits of the two flybys in the numerical model of Jia et al. (2009) along the orbits of Galileo through Ganymede's magnetosphere. The different colours show the different ULF wave activity: field line resonances are marked in red, O^+ cyclotron waves in orange, O_2^+ cyclotron waves in yellow and magnetopause waves in purple. Added to that, the magnetic field lines were traced from the wave intervals, in order to give an impression of the magnetospheric region/environment of the waves that are observed.

We have observed an harmonic spectrum of field line resonances during both flybys, when the spacecraft remained at approximately the same L-shell for 3 min around closest approach. Not all harmonics of the FLRs in Table 2 are detected above a 95 % confidence level. Especially the first harmonic in the G28 flyby is very weak. Shifting the spectrum one harmonic results in a spectrum that does not agree with the FLR model used in determining the frequencies. The amplitude of FLRs is dependent on the harmonic and on the location at which the measurements are made. The fundamental has a node at the equator (see e.g. Kivelson, 1995, Fig. 11.5), where no signal would be measured, whereas the second harmonic will have maximum amplitude at the equator. The G28 flyby was at low latitude, $-18.96°$, which may cause the weak signal at the fundamental frequency of the FLRs. Indeed, this would explain why for both low-latitude flybys the second harmonic is more significant than the fundamental. It should be mentioned that, at Mercury, Russell (1989) discussed possible FLRs where the magnetic field data only showed waves in the range of the third to fifth harmonic of the field line as would be expected near the equator.

The field line resonances that were observed near closest approach on both flybys are indicators for the plasma density near the resonant field lines. We have inferred densities of 3 and 90 AMU cm^{-3} for G8 and G28 respectively from which we calculated an ionospheric scale height of 465 km, which is much smaller that the estimate of 1000 km by Gurnett et al. (1996) but closer to the estimate of 600 km by Eviatar et al. (2001a). Similarly, the plasma temperature obtained through the magnetospheric model by Eviatar et al. (2001a) is 360 K, whereas Barth et al. (1997) found a temperature of 450 K. The reason for this discrepancy of our values and previous estimates can be found in the location of Ganymede with respect to the Jovian current sheet. The calculations we performed did not take this into account. During the G8 flyby Ganymede was near the centre of the current sheet, whereas during the G28 flyby the moon was outside the current sheet. This means that the magnetosphere for G8 was compressed compared to the G28 case. Using these two different ambient plasma cases together to determine the ionospheric scale height will then lead to an underestimate when compared with the previous estimates. Gurnett et al. (1996) and Eviatar et al. (2001a) used the G1 and G2 flybys to obtain the scale height, with both flybys in similar ambient plasma conditions as G28.

One question that has not been answered yet is what drives the FLRs. The base harmonics shown in Table 2 show that the frequency is 60 (G8) and 39 (G28) mHz for periods of 17 and 26 s. Jia et al. (2010) showed in their global model that the intermittency of the reconnection process on the magnetopause is on the order of tens of seconds. Assuming that the bursty reconnection emits compressional waves into the magnetosphere with that bursty frequency, those waves can then resonantly couple to the field lines further in and drive the FLRs that we have described (see e.g. Kivelson et al., 1998) and as described at the Earth's magnetopause by e.g. Prikryl et al. (1998).

Naturally, other sources that can drive the FLRs can be found in the dynamics of the Jovian current sheet. For example, ram pressure variations in the the upstream plasma, driven by activity in the Io plasma torus, will also interact with Ganymede's magnetosphere, and can drive

compressional waves in the magnetosphere that can again couple to resonant field lines.

Observations of ion cyclotron waves are indicative of pick-up of freshly ionized particles and have been observed around the various moons of Jupiter (see e.g. Huddleston et al., 1997; Warnecke et al., 1997; Huddleston et al., 1998; Russell et al., 2003; Volwerk et al., 2001; Volwerk and Khurana, 2010). For G8 these waves were detected just outside the magnetopause, whereas for G28 the waves were found inside the magnetosphere. This will be caused by the different conditions of the two flybys. As already mentioned before, for G8 the moon was near the centre of the Jovian current sheet and Galileo was at high northern latitude with respect to Ganymede, whereas for G28 the moon was at its highest Jovian latitude outside the current sheet and Galileo was at lower southern latitudes of Ganymede.

The ion cyclotron waves appear on open field lines with one side connected to Ganymede (G28) or on Jovian field lines (G8) outside of Ganymede's magnetosphere, which all move with respect to the moon and the pickup region. The inferred density of the pickup ions in the ring distribution on Jovian field lines at G8 is $n_r \approx 1\,\mathrm{cm}^{-3}$ for O^+, compared to the ambient plasma density in the centre of the current sheet of $n_i \approx 8\,\mathrm{cm}^{-3}$ (Kivelson, 2004, Table 21.1). For G28 the pickup occurred on open field lines and the inferred density of the pickup ions in the ring distribution was $n_r \geq 4\,\mathrm{cm}^{-3}$ for O^+ and $n_r \approx 2.5\,\mathrm{cm}^{-3}$ for O_2^+, which is significant with respect to the ambient background Jovian plasma at $n \approx 1\,\mathrm{cm}^{-3}$. However, this pickup occurs in Ganymede's magnetosphere where the density may be higher than in the Jovian current sheet. Therefore we compare the estimate of the pickup rate with the sputtering rate at the moon. The estimated pickup rates of these ions for G28 were found to be $\dot{N} \approx 5 \times 10^{23}\,\mathrm{s}^{-1}$. This rate is well below the sputtering rate of water molecules found by Paranicas et al. (1999) to be $\dot{N}_{H_2O} \sim 2 \times 10^{26}\,\mathrm{s}^{-1}$. However, Khurana et al. (2007) have shown that there is a large redeposition of the sputtered particles onto the polar cap, thereby reducing the amount of pickup that can occur significantly.

The magnetopause waves observed in the G8 flyby exhibit different characteristics on the anti-Jovian side (rotations in B_y and B_z with no compressional component) and the sub-Jovian side (rotations with strong compressional component). The amplitude of the oscillations during G8 is much larger compared with the G28 flyby. The main difference between the two flybys is the location of the moon, near the centre of the current sheet for G8 and on its outer boundary for G28. This would indicate that the plasma flow along the magnetopause is the main driver for the oscillations. However, the overall characteristics of the waves for both flybys do not seem to be in agreement with Kelvin–Helmholtz waves as one would expect. Only for the inbound crossing at G8, a case could be made looking at how the magnetic field components behave in a minimum variance coordinate system where it is found that B_m and B_n vary in phase, whereas B_l is in quadrature.

Folded flux tubes as shown by Jia et al. (2010), created by bursty reconnection on the upstream magnetopause, could provide an explanation of the wave-like perturbations observed at the magnetopause, where the flux tubes moving to the anti-Jovian side will mainly remain rotational signatures, whereas the tubes moving to the sub-Jovian side enter a slightly stronger background field and get compressed, creating the compressional signatures related to the rotations. However, this interpretation needs to be confirmed through further investigation using simulations and virtual spacecraft flybys. In Fig. 12 it is clear that the region where the magnetopause waves were observed (the purple intervals) is related to folded magnetic field lines created by reconnection. The numerical modelling by Jia et al. (2010) does not show any significant difference in the occurrence rate of the reconnection bursts between G8 and G28. There seems to be no significant difference between the two flybys in the simulations. This suggests that factors other than magnetopause reconnection need to be considered in order to fully explain the difference in the amplitude and period of the magnetic fluctuations seen during the G8 and G28 flybys.

7 Conclusions

Ganymede's mini-magnetosphere, embedded in Jupiter's larger one, shows many characteristics of "normal" magnetospheric processes, such as field line resonances and magnetopause waves. Clear indications of field line resonances were found. The boundary between Ganymede's and Jupiter's magnetospheres, the magnetopause, shows wavy activity that may be driven by the reconnection at the magnetopause, but is dependent on the density of the background plasma in which the moon is embedded. Pickup of freshly produced water-group ions and molecular oxygen has been observed through the presence of ion cyclotron waves.

The continued study of Ganymede's magnetosphere and interaction with the Jovian magnetic field using Galileo data is important with respect to the upcoming ESA L-Class mission JUICE. The results shown here can help optimize the specifications of the particles and fields instruments that will be put onto the spacecraft.

Acknowledgements. The authors would like to acknowledge the PDS/PPI for the Galileo PLS data used in this study. MV thanks Magda Delva for some useful discussions.

Topical Editor I. A. Daglis thanks P. Canu and one anonymous referee for their help in evaluating this paper.

References

Arthur, C., McPherron, R. L., and Means, J. D.: A comparitive study of three techniques for using the spectral matrix in wave analysis,

Radio Sci., 11, 833–845, 1976.
Barth, C. A., Hord, C. W., Steward, A. I. F., Pryor, W. R., Simmons, K. E., McClintock, W. E., Ajello, J. M., Naviaux, K. L., and Aiello, J. J.: Galileo ultrviolet spectrometer observations of atomic hydrogen in the atmosphere of Ganymede, Geophys. Res. Lett, 24, 2147–2150, 1997.
Bendat, J. S. and Piersol, A. G.: Measurement and analysis of random data, John Wiley & Sons, New York, USA, 1966.
Blanc, M., Alibert, Y., André, N., Atreya, S., Beebe, R., Benz, W., Bolton, S. J., Coradini, A., Coustenis, A., Dehant, V., Dougherty, M., Drossart, P., Fujimoto, M., Grasset, O., Gurvits, L., Hartogh, P., Hussmann, H., Kasaba, Y., Kivelson, M., Khurana, K., Krupp, N., Louarn, P., Lunine, J., McGrath, M., Mimoun, D., Mousis, O., Oberst, J., Pappalardo, T. O. R., Prieto-Ballesteros, O., Prieur, D., Regnier, P., Roos-Serote, M., Sasaki, S., Schubert, G., Sotin, C., Spilker, T., Takahashi, Y., Takashima, T., Tosi, F., Turrini, D., van Hoolst, T., and Zelenyi, L.: LAPLACE: A mission to Europa and the Jupiter System for ESA's Cosmic Vision Programme, Exp. Astron., 23, 849–892, 2009.
Calvin, W. M., Johnson, R. E., and Spencer, J. R.: O_2 on Ganymede: Spectral characteristics and plasma formation mechanisms, Geophys. Res. Lett., 23, 673–676, 1996.
Coates, A. J. and Jones, G. H.: Plasma environment of Jupiter family comets, Planet. Space Sci., 57, 1175–1191, 2009.
Cowee, M. M., Winske, D., Russell, C. T., and Strangeway, R. J.: 1D hybrid simulations of planetary ion-pickup: Energy partition, Geophys. Res. Lett., 34, L02113, doi:10.1029/2006GL028285, 2007.
Cummings, W. D., O'Sullivan, R. J., and Coleman, P. J.: Standing Alfvén waves in the magnetosphere, J. Geophys. Res., 74, 778–793, 1969.
Delva, M., Volwerk, M., Mazelle, C., Chaufray, J. Y., Bertaux, J. L., Zhang, T. L., and Vörös, Z.: Hydrogen in the extended Venus exosphere, Geophys. Res. Lett., 36, L01203, doi:10.1029/2008GL036164, 2008a.
Delva, M., Zhang, T. L., Volwerk, M., Vörös, Z., and Pope, S. A.: Proton cyclotron waves in the solar wind at Venus, Geophys. Res. Lett., 113, E00B06, doi:10.1029/2008JE003148, 2008b.
Dessler, A. J.: Physics of the Jovian Magnetosphere, Cambridge University Press, Cambridge, UK, 1983.
Dougherty, M. and The JUICE Science Study Team: ESA/SRE(2011)18: JUICE Exploring the emergence of habitable worlds around gas giants, ESA, Paris, France, 2011.
Eviatar, A., Lenchek, A. M., and Singer, S. F.: Distribution of density in an ion-exosphere of a nonrotating planet, Phys. Fluids, 7, 1775–1779, 1964.
Eviatar, A., Strobel, D. F., Wolven, B. C., Feldman, P. D., McGrath, M. A., and Williams, D. J.: Excitation of the Ganymede ultraviolet aurora, Astrophys. J., 555, 1013–1019, 2001a.
Eviatar, A., Vasiliũnas, V. M., and Gurnett, D. A.: The ionosphere of Ganymede, Planet. Space Sci., 49, 327–336, 2001b.
Frank, L. A., Ackerson, K. L., Lee, J. A., English, M. R., and Pickett, G. L.: the plasma instrument for the Galileo mission, Space Sci. Rev., 60, 283–307, 1992.
Frank, L. A., Paterson, W. R., Ackerson, K. L., and Bolton, S. J.: Low-energy electron measurements at Ganymede with the Galileo spacecraft: Probes of the magnetic topology, J. Geophys. Res., 24, 2159–2162, 1997.
Gary, P.: Electromagnetic ion/ion instabilities and their consequences in space plasmas: A review, Space Sci. Rev., 56, 373–415, 1991.
Gurnett, D. A., Kurth, W. S., Shaw, R. R., Roux, A., Gendrin, R., Kennel, C. F., Scarf, F. L., and Shawhan, S. D.: The Galileo plasma wave investigation, Space Sci. Rev., 60, 341–355, 1992.
Gurnett, D. A., Kurth, W. S., Roux, A., Bolton, S. J., and Kennel, C. F.: Evidence for a magnetosphere at Ganymede from plasmawave observations by the Galileo spacecraft, Nature, 384, 535–537, 1996.
Hall, D. T., Feldman, P. D., McGrath, M. A., and Strobel, D. F.: The far-ultraviolet oxygen airglow of Europa and Ganymede, Astrophys. J., 499, 475–481, 1998.
Huddleston, D. E. and Johnstone, A. D.: Relationship between wave energy and free energy from pickup ions in the comet Halley environment, J. Geophys. Res., 97, 12217–12230, 1992.
Huddleston, D. E., Strangeway, R. J., Warnecke, J., Russell, C. T., Kivelson, M. G., and Bagenal, F.: Ion cyclotron waves in the Io torus during the Galileo encounter: Warm plasma dispersion analysis, Geophys. Res. Lett., 24, 2143–2146, 1997.
Huddleston, D. E., Strangeway, R. J., Warnecke, J., Russell, C. T., and Kivelson, M. G.: Ion cyclotron waves in the Io torus: Wave dispersion, free energy analysis, and SO_2^+ source rate estimates, J. Geophys. Res., 103, 19887–19900, 1998.
Jia, X., Walker, R. J., Kivelson, M. G., Khurana, K. K., and Linker, J. A.: Properties of Ganymede's magnetosphere inferred from improved three-dimensional MHD simulations, J. Geophys. Res., 114, A09209, doi:10.1029/2009JA014375, 2009.
Jia, X., Walker, R. J., Kivelson, M. G., Khurana, K. K., and Linker, J. A.: Dynamics of Ganymede's magnetopause: Intermittent reconnection under steady external conditions, J. Geophys. Res., 115, A12202, doi:10.1029/2010JA015771, 2010.
Khurana, K. K., Pappalardo, R. T., Murphy, N., and Denk, T.: The origin of Ganymede's polar caps, Icarus, 191, 193–202, 2007.
Kivelson, M. G.: Pulsations and magnetohydrodynamic waves, in: Introduction to Space Physics, edited by: Kivelson, M. G. and Russell, C. T., pp. 330–355, Cambridge University Press, New York, 1995.
Kivelson, M. G.: Moon-magnetosphere interactions: a tutorial, Adv. Space Res., 33, 2061–2077, 2004.
Kivelson, M. G., Khurana, K. K., Means, J. D., Russell, C. T., and Snare, R. C.: The Galileo magnetic field investigation, Space Sci. Rev., 60, 357–383, 1992.
Kivelson, M. G., Khurana, K. K., Russell, C. T., Walker, R. J., Warnecke, J., Coroniti, F. V., adn D. J. Southwood, C. P., and Schubert, G.: Discovery of Ganymede's magnetic field by the Galileo spacecraft, Nature, 384, 537–541, 1996.
Kivelson, M. G., Warnecke, J., Bennett, L., Joy, S., Khurna, K. K., Linker, J. A., Russell, C. T., Walker, R. J., and Polanskey, C.: Ganymede's magnetosphere: Magnetometer overview, J. Geophys. Res., 103, 19963–19972, 1998.
Kivelson, M. G., Khurana, K. K., and Volwerk, M.: The permanent and inductive magnetic moments of Ganymede, Icarus, 157, 507–522, doi:10.1006/icar.2002.6834, 2002.
Kivelson, M. G., Bagenal, F., Kurth, W. S., Neubauer, F. M., Paranicas, C., and Saur, J.: Magnetospheric interactions with satellites, in: Jupiter: The Planet, Satellites and Magnetosphere, edited by: Bagenal, F., Dowling, T. E., and McKinnon, W. B., pp. 513–536, Cambridge University Press, Cambridge, UK, 2004.

Kurth, W. S., Gurnett, D. A., Persoon, A. M., Roux, A., Bolton, S. J., and Alexander, C. J.: The plasma wave environment of Europa, Planet. Space Sci., 49, 345–363, 2001.

Lee, M. A.: Plasma waves and instabilities at comets and in magnetospheres, AGU monograph 53, in: Ultra-low frequency waves at comets, edited by: Tsurutani, B. T. and Oya, H., pp. 13–29, AGU, Washington, D.C., USA, 1989.

Mazelle, C., Winterhalter, D., Sauer, K., Trotignon, J. G., Acuña, M. H., Baumgärtel, K., Bertucci, C., Brain, D. A., Brecht, S. H., Delva, M., Dubinin, E., Øieroset, M., and Slavin, J.: Bow shock and upstream phenomena at Mars, Space Sci. Rev., 111, 115–118, 2004.

McPherron, R. L., Russell, C. T., and Coleman, P. J.: Fluctuating magnetic fields in the magnetosphere II, ULF waves, Space Sci. Rev., 13, 411–454, 1972.

Paranicas, C., Paterson, W. R., Cheng, A. F., Mauk, B. H., McEntire, R. W., Frank, L. A., and Williams, D. J.: Energetic particle observations near Ganymede, J. Geophys. Res., 104, 17459–17469, 1999.

Paterson, W. R., Frank, L. A., and Ackerson, K. L.: Galileo plasma observations at Europa: Ion energy spectra and moments, J. Geophys. Res., 104, 22779–22791, 1999.

Prikryl, P., Greenwald, R. A., Sofko, G. J., Villain, J. P., Ziesolleck, C. W. S., and Friis-Christensen, E.: Solar-wind-driven pulsed magnetic reconnection at the dayside magnetopause, Pc5 compressional oscillations, and field line resonances, J. Geophys. Res., 103, 17307–17322, 1998.

Russell, C. T.: ULF waves in the Mercury magnetosphere, Geophys. Res. Lett., 16, 1253–1256, 1989.

Russell, C. T., Blanco-Cano, X., Wang, Y. L., and Kivelson, M. G.: Ion cyclotron waves at Io: implications for the temporal variation of Io's atmosphere, Planet. Space Sci., 51, 937–944, 2003.

Sonnerup, B. U. Ö. and Scheible, M.: Minimum and maximum variance analysis, in: Analysis Methods for Multi-Spacecraft Data, edited by: Paschmann, G. and Daly, P., pp. 185–220, ESA, Noordwijk, 1998.

Vasiliũnas, V. M. and Eviatar, A.: Outflow of ions from Ganymede: A reinterpretation, Geophys. Res. Lett., 27, 1347–1349, 2000.

Volwerk, M. and Khurana, K. K.: Ion pick-up near the icy Galilean satellites, in: Pickup ions throughout the heliosphere and beyond, AIP conference proceedings, Vol. 1302, edited by: le Roux, J. A., Florinski, V., and Zank, G. P., pp. 263–269, IAP, Melville, NY, USA, 2010.

Volwerk, M., Kivelson, M. G., and Khurana, K. K.: Probing Ganymede's magnetosphere with field line resonances, J. Geophys. Res., 104, 14729–14738, 1999.

Volwerk, M., Kivelson, M. G., and Khurana, K. K.: Wave activity in Europa's wake: Implications for ion pick-up, J. Geophys. Res., 106, 26033–26048, 2001.

Warnecke, J., Kivelson, M. G., Khurana, K. K., Huddleston, D. E., and Russell, C. T.: Ion cyclotron waves observed at Galileo's Io encounter: Implications for neutral cloud distribution and plasma composition, Geophys. Res. Lett., 24, 2139–2142, 1997.

Williams, D. J.: Ganymede's ionic radiation belts, Geophys. Res. Lett., 28, 3793–3796, 2001.

Williams, D. J.: Energetic electron beams in Ganymede's magnetosphere, J. Geophys. Res., 109, A09211, doi:10.1029/2004JA010521, 2004.

Williams, D. J., McEntire, R. W., Jaskulek, S., and Wilken, B.: The Galileo energetic particle detector, Space Sci. Rev., 60, 385–412, 1992.

Williams, D. J., Mauk, B., and McEntire, R. W.: Trapped electrons in Ganymede's magnetic field, Geophys. Res. Lett., 24, 2953–2956, 1997a.

Williams, D. J., Mauk, B. H., McEntire, R. W., Roelof, E. C., Armstrong, T. P., Wilken, B., Roederer, J. G., Krimigis, S. M., Fritz, T. A., Lanzerotti, L. J., and Murphy, N.: Energetic particle signatures at Ganymede: Implications for Ganymede's magnetic field, Geophys. Res. Lett., 24, 2163–2166, 1997b.

Williams, D. J., Mauk, B., and McEntire, R. W.: Properties of Ganymede's magnetosphere as revealed by energetic particle observations, J. Geophys. Res., 103, 17526–17534, 1998.